The Astronomical Journal, 132:1316–1321, 2006 September

PROTOPLANET DYNAMICS IN A SHEAR-DOMINATED DISK

Benjamin F. Collins and Re'em Sari
California Institute of Technology, MC 130-33, Pasadena, CA 91125; bfc@tapir.caltech.edu
Received 2006 March 23; accepted 2006 June 1

ABSTRACT

The velocity dispersion, or eccentricity distribution, of protoplanets interacting with planetesimals is set by a balance between dynamical friction and viscous stirring. We calculate analytically the eccentricity distribution function of protoplanets embedded in a cold, shear-dominated planetesimal swarm. We find a distinctly non-Rayleigh distribution with a simple analytical form. The peak of the distribution lies much lower than the rms value, indicating that while most of the bodies have similarly small eccentricities, a small subset of the population contains most of the thermal energy. We also measure the shear-dominated eccentricity distribution using numerical simulations. The numerical code treats each protoplanet explicitly and adds an additional force term to each body to represent the dynamical friction of the planetesimals. Without fitting any parameters, the eccentricity distribution of protoplanets in the *N*-body simulation agrees with the analytical results. This distribution function provides a useful tool for testing hybrid numerical simulations of late-stage planet formation.

Key words: planets and satellites: formation — solar system: formation

1. INTRODUCTION

Terrestrial planets, ice giants, and the cores of gas giants are thought to form by accretion of planetesimals into protoplanets. The protoplanets emerge from the swarm of planetesimals after an epoch of runaway accretion. The subsequent dynamics of the protoplanets sets several important features of the final planetary configuration, such as the mass and number of planets or cores. It is difficult to constrain this evolution, however, without constraining the properties of the disk in which they are embedded.

One important yet uncertain parameter is the size of the planetesimals, the building blocks. The outer solar system and the later stages of formation in the inner solar system likely lack gas, allowing the formation of kilometer-size bodies through gravitational instabilities. Those bodies collide and grind each other down to even smaller sizes in a collisional cascade. The existence of bodies small enough to damp their own velocity dispersion is an inevitable conclusion from the existence of Uranus and Neptune (Goldreich et al. 2004b). Without such small bodies, the ability of a growing protoplanet to gravitationally focus the planetesimals becomes inefficient, and the growth timescale becomes too long, of order 10^{12} yr in the outer solar system.

The unavoidable influence of the planetesimals makes numerical studies of planet formation difficult to carry out accurately. Despite modern computational power, an integration of the equations of motion for each body in a protoplanet and planetesimal swarm is impossible. Even without allowing planetesimal fragmentation, the number of kilometer-size bodies needed to compose a Neptune-size mass is humongous, of order 10^{12}. Kokubo & Ida (1996) performed numerically feasible but physically less appropriate *N*-body simulations of a protoplanetary disk in which the sizes of the planetesimals were larger than the value required to form the ice giants of our solar system. Although interesting from a dynamical viewpoint, the results of such simulations cannot be extrapolated to the scenario of smaller planetesimals, since they lack collisional damping.

An alternative numerical approach to studying these systems is a coagulation code (Lee 2000; Kenyon & Luu 1998) in which the bodies are divided into size bins and the interaction of each pair of bins is calculated statistically. This approach fails once the number of bodies in any bin is not sufficiently large. Kenyon & Bromley (2006) have developed a hybrid code that treats planetesimals statistically while a small number of large bodies are integrated individually.

In this paper we examine the processes that shape the eccentricity distribution of the large bodies. We assume, simply, that the planetesimals constitute a cold disk due to sufficiently frequent collisions. As a first step, we include the dynamical friction that the planetesimals exert on the large bodies but ignore the much slower process of their accretion onto those bodies. The rates of cooling from dynamical friction and heating from mutual excitations are discussed in § 2. We write a Boltzmann equation to show the change in the distribution function of eccentricities due to each process in § 3, and we discuss the solution to that equation. In § 4 we present the results of complementary *N*-body simulations designed to measure the eccentricity distribution directly. A discussion of the results follows in § 5.

2. SHEAR-DOMINATED COOLING AND HEATING RATES

The eccentricities of the protoplanets represent a kind of "thermal" energy in their orbits, relative to perfectly circular motion. The extra noncircular velocity itself varies in magnitude and direction over an orbital period; it is simpler to use the eccentricity, a constant of motion for the two-body problem. Specifically, we calculate the vector eccentricity,

$$\boldsymbol{e} = \frac{\boldsymbol{v} \times \boldsymbol{H}}{GM_p} - \hat{\boldsymbol{r}}. \tag{1}$$

This expression relates the eccentricity of the particle, $\boldsymbol{e}$, to the particle's position, $\boldsymbol{r}$, its velocity, $\boldsymbol{v}$, its orbital angular momentum vector, $\boldsymbol{H}$, and its mass, M_p. In general, a protoplanet can have an inclination relative to the disk plane, and the eccentricity vector can have three components. However, we show in § 2.4 that the shear-dominated regime strongly inhibits the growth of inclinations. Two dimensions then suffice to describe the configuration space of $\boldsymbol{e}$.

We use the quantity of the Hill radius repeatedly in this work; for reference we define its value as

$$R_{\rm H} \equiv \left(\frac{M_p}{3\ M_\odot}\right)^{1/3} a = \frac{R}{\alpha}, \tag{2}$$

where M_p is the mass of a particle, a is its semimajor axis, R is its radius, ρ is its mean density, and

$$\alpha = \left(\frac{3\ M_\odot}{M_p}\right)^{1/3} \frac{R}{a} = \left(\frac{3\rho_\odot}{\rho}\right)^{1/3} \frac{R_\odot}{a}. \tag{3}$$

The Hill radius, in turn, specifies an eccentricity, the Hill eccentricity:

$$e_{\rm H} = R_{\rm H}/a. \tag{4}$$

We restrict this study to disks in which the majority of the bodies have eccentricities lower than $e_{\rm H}$, known as "the shear-dominated regime."

For most of this paper we employ the "two groups" approximation (Wetherill & Stewart 1989; Goldreich et al. 2004b) and split the disk into two uniform populations. One group is the numerous smaller bodies, or "planetesimals." We denote their surface mass density as σ. The other group, the "protoplanets," consists of the bodies that dominate the excitations of the disk particles. Each protoplanet has a radius R, mass M, mean density ρ, and eccentricity e. We write the total surface mass density in protoplanets as Σ. We assume that $\sigma > \Sigma$, which keeps the protoplanets in the shear-dominated regime. It is likely that the violation of this assumption due to the growth of the protoplanets begins the final stages of planet formation (Goldreich et al. 2004a).

2.1. *Eccentricity Excitation of Protoplanets*

We analyze the interaction of two protoplanets from a frame rotating with a reference orbit at a semimajor axis a. The difference between the Keplerian angular velocity at each radius induces a shearing motion between particles on nearby circular orbits. For an orbit interior to a by a distance b,

$$\Omega_{\rm rel}(b) = \Omega(a+b) - \Omega(a) \approx \frac{3}{2}\Omega\frac{b}{a}, \tag{5}$$

in the limit of $b \ll a$. This angular frequency also specifies the rate of conjunctions for the two bodies with orbits separated by b.

The change in their eccentricity from each conjunction can be calculated analytically for two nearly circular orbits when $b \gg R_{\rm H}$:

$$e_k = A_k e_{\rm H}\left(\frac{b}{R_{\rm H}}\right)^{-2}, \tag{6}$$

$$A_k = \frac{16}{3}\left[K_0\left(\frac{2}{3}\right) + \frac{1}{2}K_1\left(\frac{2}{3}\right)\right] \approx 6.7. \tag{7}$$

Here K_0 and K_1 are modified Bessel functions of the second kind (Goldreich & Tremaine 1980; Petit & Henon 1986; Duncan et al. 1989). We note that e_k refers to the perturbed body, while $e_{\rm H}$ and $R_{\rm H}$ refer to the Hill parameters of the perturbing body. The kick, viewed as a change in the eccentricity vector, is independent of the original eccentricity of the particle. Its orientation is perpendicular to the line connecting the two protoplanets and the Sun at conjunction; we therefore assume it is random.

The eccentricity kick given by one protoplanet is strongest for the particles that approach with an impact parameter on the order of the Hill radius. Interactions from a greater distance, however, occur more often. In a shear-dominated disk, eccentricities are small, $e \ll e_{\rm H}$; to change that eccentricity significantly only requires small perturbations. These frequent but weaker perturbations dictate the overall velocity evolution of the protoplanets (Goldreich et al. 2004b; Rafikov 2004).

Specifically, the average differential rate at which one protoplanet receives eccentricity kicks of strength e from other protoplanets is given by

$$d\mathcal{R}_{\rm ex}(e) = 2n_{\rm big}\frac{3}{2}\Omega b(e)\frac{db}{de}\,de, \tag{8}$$

where $n_{\rm big}$ is the number surface density of protoplanets and $\frac{3}{2}\Omega b(e)$ is the velocity of encounters at those separations (given by eq. [5]). The factor of 2 accounts for the combination of interior and exterior encounters. The excitation rate of a protoplanet with eccentricity e is then the rate of kicks comparable in magnitude to its current eccentricity:

$$\left.\frac{1}{e}\frac{de}{dt}\right|_{\rm ex} \sim e\left|\frac{d\mathcal{R}_{\rm ex}(e)}{de}\right| \sim \frac{\Sigma\Omega}{\rho R}\frac{1}{\alpha^2}\frac{e_{\rm H}}{e}. \tag{9}$$

The inverse of this rate can be interpreted as the timescale for a protoplanet's eccentricity to change by an amount e.

2.2. *Dynamical Friction*

As each protoplanet moves through the disk, it scatters and excites the eccentricities of the planetesimals that surround it. Cold planetesimals that approach a protoplanet with impact parameters of about a Hill radius leave with $\sim me_{\rm H}$ of additional momentum. This can either add to or subtract from the eccentricity of the protoplanet, depending on the relative orientation between the preencounter eccentricities of the protoplanet and planetesimal. We write the net effect (Goldreich et al. 2004b),

$$M\frac{de}{dt} \sim -n_s R_{\rm H} e_{\rm H} m(e_{\rm H}+e) + n_s R_{\rm H} e_{\rm H} m(e_{\rm H}-e), \tag{10}$$

for a number surface density of planetesimals n_s. This formula yields the damping rate, or the inverse damping time,

$$\tau_d^{-1} \equiv -\left.\frac{1}{e}\frac{de}{dt}\right|_{\rm df} = C_d\frac{\sigma\Omega}{\rho R}\frac{1}{\alpha^2}. \tag{11}$$

Calculating the coefficient C_d requires a more precise analysis of planetesimal scattering. We adopt the value $C_d \approx 10$ found by Ohtsuki et al. (2002), who measure the coefficient numerically.

2.3. *Planetesimal Interactions*

The distribution of planetesimal eccentricities does not affect our results, as neither the excitation nor the damping rates depend on their eccentricity as long as the planetesimals remain in a shear-dominated state. In this work we focus on a range of parameters such that collisional cooling keeps the eccentricities of planetesimals below $e_{\rm H}$ and enforces the condition of shear domination.

2.4. *Inclinations*

An orbit with a small inclination angle i carries its particle out of the disk plane on vertical excursions of size $\sim ia$. An interaction that excites that particle's eccentricity also affects its

inclination, but with a magnitude inhibited by the geometry of the distant encounter,

$$\frac{i_k}{e_k} \sim \frac{ai}{b} \Rightarrow \frac{i_k}{i} \sim \left(\frac{e}{e_{\rm H}}\right)^{3/2} \frac{e_k}{e}, \quad (12)$$

where b is the impact parameter of the perturber and i_k is the resulting change in inclination from an encounter. In contrast, planetesimals just entering the Hill sphere of a protoplanet damp the protoplanet's noncircular velocity in all dimensions; no equivalent geometric factor inhibits the damping of inclinations. With the growth of inclinations suppressed, shear-dominated protoplanet disks are effectively two-dimensional (Wetherill & Stewart 1993; Goldreich et al. 2004b; Rafikov 2003).

2.5. *The Eccentricity Distribution: A Qualitative Discussion*

The dynamical friction rate sets a characteristic time over which the eccentricities of all of the bodies are changed significantly. In this sense, the eccentricity distribution of the protoplanetary swarm is reset every τ_d. The excitation rate, however, varies with e. Equating the excitation rate, equation (9), and the damping rate, equation (11), yields an important reference value, $e_{\rm eq}$:

$$e_{\rm eq} \sim \frac{\Sigma}{\sigma} e_{\rm H}. \quad (13)$$

Statistically, each protoplanet receives one kick of this magnitude every damping timescale. We note that our restriction to disks in which $\sigma > \Sigma$ enforces the condition that $e_{\rm eq} < e_{\rm H}$, or that the planetesimal damping effectively balances the protoplanet stirring.

We deduce the distribution of eccentricities on each side of $e_{\rm eq}$ by examining the dependence of the kicking rate on eccentricity. Excitation to $e \gg e_{\rm eq}$ requires a kick $e_k \gg e_{\rm eq}$. Such strong kicks occur less often in one damping timescale than kicks of strength $e_{\rm eq}$ by a factor of $e_{\rm eq}/e_k$. With fewer kicks to populate the high-eccentricity distribution, the number of bodies with such eccentricities echoes the rate of kicks and falls off with eccentricity as e^{-1} (Goldreich et al. 2004b).

Kicks of order $e \ll e_{\rm eq}$ occur frequently in each damping timescale, thereby overwhelming the effects of dynamical friction on the lowest eccentricity bodies. A dynamic equilibrium dominated by only the stirring mechanism implies that kicks to and from every eccentricity vector occur at the same rate. For this to be true the distribution must be constant over the configuration space. The number of bodies with an eccentricity of order $e \ll e_{\rm eq}$ then scales as the area of configuration space available, $\sim e^2$.

3. A BOLTZMANN EQUATION

In this section we develop a differential equation to describe analytically the distribution function of protoplanet eccentricities. We construct this equation in the spirit of the Boltzmann equation, examining the change in the number of bodies with a particular eccentricity due to the effects of dynamical friction and viscous stirring.

The space of possible eccentricities is inherently two-dimensional (eq. [1]), since inclinations can be neglected (§ 2.4). In addition, the interaction rates depend only on the magnitude of the protoplanet eccentricity, forcing the distribution function to share this dependence: $f(\boldsymbol{e}) = f(e)$. The two-dimensional $f(e)$ is related to the number of bodies with velocity on the order of e by its integral, roughly $e^2 f(e)$.

Dynamical friction lowers the eccentricities of all bodies proportionally to their eccentricity. Equivalently, the number of bodies with a certain e changes as the protoplanets with that value are damped to lower eccentricities and replaced by bodies from a higher eccentricity. We write this as

$$\left.\frac{\partial f(e)}{\partial t}\right|_{\rm df} = -{\rm div}\left[f(e)\frac{\partial \boldsymbol{e}}{\partial t}\right] = \frac{\partial f(e)}{\partial e}\frac{e}{\tau_d} + \frac{2f(e)}{\tau_d}, \quad (14)$$

where we have used $\partial \boldsymbol{e}/\partial t = -\boldsymbol{e}/\tau_d$ for the effects of dynamical friction.

At a given $\boldsymbol{e}$, particles are kicked to a new eccentricity $\boldsymbol{e}_n$ at an average rate that depends on the magnitude of the kick, $|\boldsymbol{e}_n - \boldsymbol{e}|$. Also, particles with an initial eccentricity $\boldsymbol{e}_n$ are kicked to $\boldsymbol{e}$ at the same rate. The total flux of particles to and from a given eccentricity is

$$\left.\frac{\partial f(e)}{\partial t}\right|_{\rm kicks} = \int\int p(|\boldsymbol{e}_n - \boldsymbol{e}|)[f(e_n) - f(e)]\, d^2\boldsymbol{e}_n, \quad (15)$$

where $p(e)$ describes the rate at which bodies experience changes in their eccentricities by an amount e. This is the two-dimensional analog of the excitation rate equation (9):

$$p(e) = \frac{1}{2\pi e}\left|\frac{\partial \mathcal{R}_{\rm ex}}{\partial e}\right| = A_k \frac{9}{16\pi^2}\frac{\Sigma\Omega}{\rho R}\frac{1}{\alpha^2} e_{\rm H}\frac{1}{e^3}. \quad (16)$$

The sum of the dynamical friction terms and the kicking integral describes the dynamics of shear-dominated protoplanets interacting with each other in a smooth disk of planetesimals. The combined influence of these two processes can bring the protoplanets into an equilibrium state, where the number of particles with eccentricity $\boldsymbol{e}$ remains constant in time:

$$0 = \frac{\partial f(e)}{\partial e}\frac{e}{\tau_d} + \frac{2f(e)}{\tau_d} + \int\int p(|\boldsymbol{e}_n - \boldsymbol{e}|)[f(e_n) - f(e)]\, d^2\boldsymbol{e}_n. \quad (17)$$

3.1. *The Solution*

We show in the Appendix that

$$f(e) = \frac{1}{2\pi e_*^2}\left[1 + \left(\frac{e}{e_*}\right)^2\right]^{-3/2}, \quad (18)$$

$$e_* = \frac{9A_k}{8\pi C_d} e_{\rm eq} \approx 0.24\frac{\Sigma}{\sigma} e_{\rm H}$$

satisfy the equilibrium equation, equation (17), for all e. This function is the equilibrium eccentricity distribution of shear-dominated protoplanets.

Figure 1 (*solid line*) shows a distribution function for $\Sigma \approx 0.002$ g cm^{-2} and $\sigma = 0.1$ g cm^{-2}. Although the function formally extends above $e_{\rm H}$, we stress that it is only accurate for eccentricities $e \ll e_{\rm H}$. Both the dynamical friction and the excitation rates (eqs. [14] and [16]) are not valid for $e \gtrsim e_{\rm H}$.

Several moments of the distribution can be calculated in terms of the only free parameters:

$$\frac{e_{\rm median}}{e_{\rm H}} = 0.41\frac{\Sigma}{\sigma}, \frac{\langle e\rangle}{e_{\rm H}} = 0.24\frac{\Sigma}{\sigma}\log\left(3\frac{\sigma}{\Sigma}\right), \frac{\langle 1/e\rangle^{-1}}{e_{\rm H}} = 0.24\frac{\Sigma}{\sigma}. \quad (19)$$

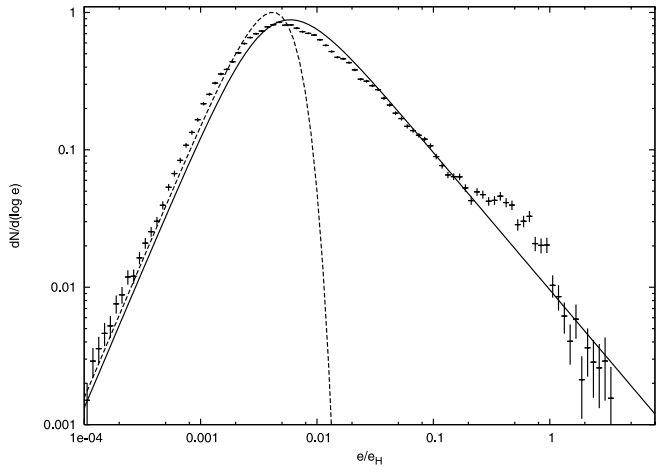

FIG. 1.— Plot of eq. (18) superposed on the results of a numerical simulation. The simulated disk contains 120 bodies of mass $M = 5 \times 10^{24}$ g, or $\Sigma \approx 0.002$ g cm^{-2}. A planetesimal surface density of $\sigma = 0.1$ g cm^{-2} is included. We assume that each bin obeys Poisson statistics and assign errors based on a population size of $N_b N_{\tau_d}$, where N_b is the number of bodies in the simulation and N_{τ_d} is the total measurement time in units of damping timescales. The solid line shows the distribution as given by eq. (18), using the same values of Σ and σ. A Rayleigh distribution with a similar peak eccentricity is plotted with the dashed line.

According to equation (18), $\langle e \rangle$ is infinite. However, the largest single kick in eccentricity from an almost circular protoplanet encounter is of order $e_{\rm H}$. Truncating the integral at $e_{\rm H}$ produces the logarithmic term in the expression above. Moments higher than the mean also diverge; realistically, they are dominated by the bodies with the highest eccentricities, of order $e_{\rm H}$.

It is easy to see that this solution, in the high- and low-eccentricity limits, produces the same power laws discussed in § 2.5. In fact, it can be shown directly from equation (17) that any solution to this differential equation reduces to those limiting power laws.

4. NUMERICAL SIMULATIONS

Here we describe a direct measurement of the eccentricity distribution from gravitational N-body simulations that include an additional force to represent dynamical friction.

The N-body part of our simulation uses Gauss's equations to evolve a set of orbital constants chosen to vary slowly under small perturbations. A modified version of Kepler's equation produces the orbital phase for each body at each time step. The IDA solver from the SUNDIALS software package (Hindmarsh et al. 2005) integrates the dynamical equations. During close encounters of two protoplanets, we integrate their motion relative to the center of mass of the pair.

We represent the planetesimal population in these simulations with an extra force term that damps the noncircular velocities of the protoplanets at the rate $\mathcal{R}_d(e)$, given by equation (11). An ad hoc transition between the damping rate for $e < e_{\rm H}$ and the appropriate rate for $e > e_{\rm H}$ prevents unphysical enhancements of the damping force during close encounters. The growth of protoplanets in mass due to planetesimal accretion is not included; the accretion rate is always lower than the dynamical friction rate and will not affect the eccentricity evolution (Goldreich et al. 2004b).

Each simulation begins with the protoplanets on circular orbits with random phases and random semimajor axes within a chosen annulus. The average spacing between bodies, $M/(\Sigma 2\pi a)$, is several Hill radii. The protoplanets interact for several damping timescales τ_d before the distribution reaches equilibrium.

We record the eccentricity of the protoplanets every $\Delta t \approx 0.1\tau_d$ starting at about $100\tau_d$. The bodies in the inner and outer edges of the disk are not measured, in order to avoid artificial boundary effects that inhibit excitations. We bin all of the measured eccentricities logarithmically; a well-populated histogram is produced with several hundred orbits of measurement. Errors are assigned to each bin according to a Poisson distribution, with the sample size defined as the product of the number of bodies measured and the sampling time in units of the damping timescale τ_d. Since each protoplanet suffers a significant change in eccentricity every τ_d, one measurement of the eccentricity distribution is independent from a previous measurement if they are separated in time by τ_d. We sample faster than τ_d to increase the resolution of the histogram slightly.

The statistical error bars do not take into account the inhomogeneity of the protoplanet disk on small length scales. Given a surface density, the mass of a single protoplanet sets a typical radial separation between bodies. This length scale corresponds to an eccentricity scale through equation (6) (in the simulations presented here, this value is slightly below $e_{\rm H}$). As the disk evolves, the viscous stirring causes migrations in the semimajor axes of the particles that smooth the average radial distribution. If measured only over intervals shorter than the migration timescale, the eccentricity distribution may vary for eccentricities above the eccentricity set by the typical separation. Fluctuations from this effect are visible in Figures 1 and 2.

Several simulations of disks with different protoplanet mass distributions are presented in §§ 4.1 and 4.2.

4.1. *Equal-Mass Protoplanets*

Figure 1 shows the eccentricity distribution measured from a simulated disk of 120 equal-mass protoplanets ($M = 2.5 \times 10^{-9}\ M_\odot$) with surface densities $\Sigma \approx 0.002$ g cm^{-2} and $\sigma = 0.1$ g cm^{-2}. A single population of protoplanets best reflects the "two groups" approximation we use to derive equations (9) and (11). The analytic solution, equation (18), for the same parameters in the simulation is superposed in Figure 1. While the overall match is not perfect, the shape of each curve is strikingly similar. The two curves match extremely well if one is shifted by around 15% in the e-direction. This difference is attributable to the difficulty of assigning a correct value of Σ to the simulation given a finite number of protoplanets.

We note that there are no free parameters in this comparison. The numerical distribution is a direct counting of the number of bodies within each eccentricity bin, while a choice of Σ, σ, and M completely specifies the analytical curve.

4.2. *Mass Distributions*

Naturally occurring protoplanet populations exhibit nontrivial distributions in mass. Before describing such a disk in the framework we have developed, we clarify several points.

Protoplanets with different masses or, equivalently, different radii experience different viscous stirring rates. We decompose the total surface density in protoplanets, Σ, into a differential quantity, $d\Sigma/dR$, and write the excitation rate of a body with radius R as

$$\mathcal{R}_x(e, R) \sim \int \frac{d\Sigma}{dR'} \frac{\Omega}{\rho R'} \frac{1}{\alpha^2} \frac{e_{\rm H}(R')}{e}\, dR'. \qquad (20)$$

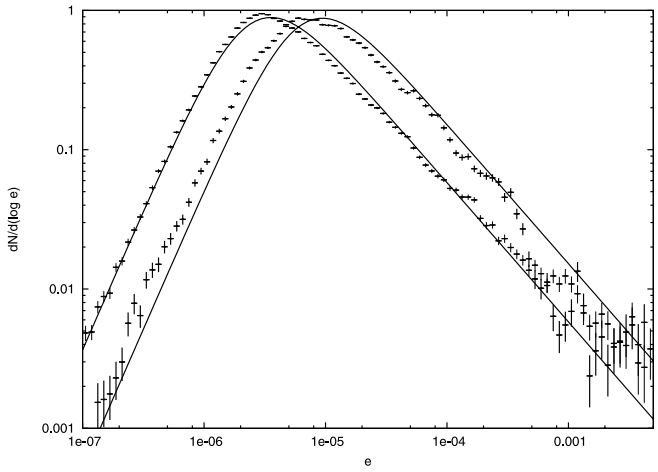

FIG. 2.—Comparison of the results of a numerical simulation of protoplanets in a perfectly bimodal mass distribution ($m_1 = 2 \times 10^{24}$ g, $m_2 = 3.8 \times 10^{25}$ g). We simulate 60 bodies of each mass, for a total surface density in protoplanets of $\Sigma \approx 0.003$ g cm^{-2} and a planetesimal surface density of $\sigma = 0.2$ g cm^{-2}. The eccentricities of each mass group are binned separately; each distribution is a good match to eq. (18) when scaled to the appropriate Hill eccentricity. The distribution for bodies of mass m_1 therefore peaks on the left, and the distribution for the higher mass bodies peaks on the right. The error bars are assigned following the same algorithm as in Fig. 1.

The identity $e_{\rm H}(R') = (R'/R)e_{\rm H}(R)$ when substituted into equation (20) yields

$$\mathcal{R}_x(e, R) \sim \frac{\Omega}{\rho R}\frac{1}{\alpha^2}\frac{e_{\rm H}(R)}{e}\int \frac{d\Sigma}{dR'}\, dR'. \tag{21}$$

In words, the excitation rate of one body only depends on the total surface density of all other bodies, regardless of the specific mass distribution. This differs from the assertion by Goldreich et al. (2004b) that only the most massive bodies contribute to the viscous stirring rate. Equation (21) seems to indicate that there should be no distinction between big bodies and small bodies, since every body contributes to the viscous stirring. A closer investigation uncovers the mass range of bodies that provide significant stirring.

Eccentricity kicks of strength e_k can occur at any combination of M and b that satisfies the inverse-square law of gravitation: $e_k \sim M(R')b(R')^{-2}$. However, the smallest impact parameter that contributes to a body's excitation is about $R_{\rm H}$. A minimum $b(R') \sim R_{\rm H}$ sets a minimum mass for bodies to kick a body with mass M by an amount e_k:

$$M_{\rm min}(e_k, R) \sim \frac{e_k}{e_{\rm H}} M. \tag{22}$$

Likewise, a body can only be as far away as its radial position in the disk, a. This sets a maximum mass,

$$M_{\rm max}(e_k, R) \sim \left(\frac{e_k}{e_{\rm H}} M\right)\frac{a^2}{R_{\rm H}^2}. \tag{23}$$

For a choice of the most relevant kick strength, e_k, these limits define the sizes of bodies that participate in the excitation of a body with size R.

As a numerical confirmation of these results, we simulate a disk of planetesimals with a surface mass density $\sigma = 0.2$ g cm^{-2} and 120 protoplanets. In this case we divide the protoplanets into two groups of different mass: 60 of mass $m_1 = 2 \times 10^{24}$ g and 60 of mass $m_2 = 3.8 \times 10^{25}$ g. These masses are within the limits set by equations (22) and (23). We plot the absolute eccentricity distribution of each mass group binned separately in Figure 2. In addition, we plot the analytic distributions given by σ, as specified above, and Σ, the sum of the surface densities of both groups.

It is clear that each group of protoplanets with the same mass matches the analytic distribution well. The offset between the peak of each group is due to the dependence of the distribution on the Hill eccentricity of each body. In general, the distribution for a swarm of protoplanets with a mass distribution is merely the sum of individual distributions for protoplanets of each mass.

5. CONCLUSIONS

We present an analytic model for the distribution function of the eccentricities of a protoplanet population embedded in a shear-dominated planetesimal disk. The eccentricity distribution measured with numerical simulations matches the analytical result very well.

Since we have manually inserted the dynamical friction rate that we expect into the numerical simulations, this work does not test our prescription of dynamical friction. However, the numerical and analytic representations of viscous stirring are completely independent. Equation (17) uses a viscous stirring rate that includes only distant encounters. In our numerical simulations, Newton's laws dictate the protoplanet interactions directly without any simplifying assumptions. The consistency of the two calculations proves that in a two-dimensional shear-dominated disk, interactions between noncrossing orbits are entirely responsible for setting the eccentricities of the protoplanets.

Several features of the distribution highlight interesting properties of the dynamics. We reason in § 2.5 that most protoplanets have eccentricities $\sim(\Sigma/\sigma)e_{\rm H}$, the value at which the excitation and damping timescales are equal. The distribution function shows this to be true: the median and mean (up to a logarithmic factor) of any distribution are on the order of this equilibrium eccentricity. Higher moments of the distribution are dominated by the highest eccentricity bodies. These differences signal that different statistics of the distribution can reflect different subsets of the overall population. For example, the average "thermal" energy of the protoplanets is represented by their rms eccentricity, $\langle e^2 \rangle$. The fractionally fewer bodies with eccentricities close to $e_{\rm H}$ dominate $\langle e^2 \rangle$ and thus contain most of the energy.

The shape of the distribution also merits discussion. The N-body integrations of a group of single-mass bodies show that their eccentricities follow a Rayleigh distribution (Ida & Makino 1992). For reference, we plot a Rayleigh distribution in Figure 1. It is entirely inconsistent with our calculations. This is not surprising. In addition to simulating bodies in the regime of eccentricities that are large compared to the Hill eccentricity, Ida & Makino (1992) do not include any effects that can balance the mutual excitations of their particles. The dynamical friction in our simulations balances the viscous stirring and establishes the equilibrium distribution we derive.

Since the accretion timescale is much longer than the dynamical timescale, the balance between eccentricity excitation and damping is maintained as Σ grows relative to σ. The peak of the distribution, set by Σ/σ, mirrors this growth and moves closer to $e_{\rm H}$; the shape remains the same. Our assumptions fail, however, when $\Sigma \sim \sigma$. At this epoch, the typical velocities are close to $e_{\rm H}$ and the disk is no longer shear-dominated. In addition, the damping rate can no longer balance the viscous stirring rate, and the eccentricities of the protoplanets grow. The chaotic evolution that

follows likely sets the final spacing and number of members of the resulting solar system (Goldreich et al. 2004a).

It is possible to extend this result to other scenarios. One situation with the same dynamics is that of planetesimals in the outer solar system in the presence of a gaseous disk. When the mean free path of the gas is long compared to the radius of a planetesimal, the damping timescale for the eccentricity of the planetesimals is constant. Assuming again that the disk is shear-dominated with respect to a population of larger protoplanets, those protoplanets excite the planetesimals through the same non-orbit-crossing interactions discussed in § 2.1. With a known distribution function, the average rate of catastrophic collisions can be calculated even when a typical body does not have enough energy for significant fragmentation. A collisional cascade to smaller planetesimals is crucial for the rapid growth of the protoplanetary cores necessary to form Uranus and Neptune (Goldreich et al. 2004b; Rafikov 2004).

We thank Scott Kenyon and the anonymous referee for their useful comments. R. S. is an Alfred P. Sloan Fellow and a Packard Fellow.

APPENDIX

THE ANALYTIC DISTRIBUTION FUNCTION

Here we outline the evaluation of the equilibrium equation, equation (17), using the distribution function, equation (18). To simplify the notation, we rescale all eccentricities by e_* and algebraically manipulate the coefficients of each term in equation (17). We are left with the equivalent burden of proving that

$$g(e) = (1 + e^2)^{-3/2} \tag{A1}$$

satisfies

$$2\pi \frac{\partial g(e)}{\partial e} e + 4\pi g(e) = \int\int \frac{g(e) - g(e_n)}{|\boldsymbol{e}_n - \boldsymbol{e}|^3}\, d^2\boldsymbol{e}_n. \tag{A2}$$

The left-hand side is easy to compute:

$$2\pi \frac{\partial g(e)}{\partial e} e + 4\pi g(e) = \frac{4\pi}{(1 + e^2)^{3/2}} - \frac{6\pi e^2}{(1 + e^2)^{5/2}}. \tag{A3}$$

To integrate the right-hand side, we translate the origin of the integration variables by $\boldsymbol{e}$ and rotate them to align $\boldsymbol{e}$ with one of the coordinate axes. In those coordinates,

$$I = \int_{-\infty}^{\infty}\int_{-\infty}^{\infty} \frac{1}{(k^2 + h^2)^{3/2}} \left\{ \frac{1}{(1 + e^2)^{3/2}} - \frac{1}{\left[1 + k^2 + (h + e)^2\right]^{3/2}} \right\} dk\, dh, \tag{A4}$$

with $\boldsymbol{e}_n = \{k, h\}$.

After the integration over k, we rewrite the integral in terms of a new variable $h' \equiv (1 + e^2)/(eh)$,

$$I = \int_{-\infty}^{\infty} \left\{ \frac{2e}{(1 + e^2)^{5/2}} + \frac{8}{(1 + e^2)^2} \frac{\partial^2 E[e^2 z/(1 + e^2)]}{\partial z^2} |h'| h'^2 \right\} dh', \tag{A5}$$

where $z = -2h' - h'^2$ and $E[e^2 z/(1 + e^2)]$ is the complete elliptic integral of the second kind.

We change the integration variable to z, taking care to evaluate the integrand with the appropriate branch of the double-valued relation $h'(z)$. The integral evaluates to

$$I = \frac{4\pi}{(1 + e^2)^3} + \frac{8}{(1 + e^2)^2} \int_0^1 \left(\frac{4 - 3z}{\sqrt{1 - z}} \right) \frac{\partial^2 E[e^2 z/(1 + e^2)]}{\partial z^2}\, dz. \tag{A6}$$

With the second derivative of the elliptic function expressed as a power series, each term can be integrated over z. The remaining power series in $e^2/(1 + e^2)$ equals

$$I = \frac{4\pi}{(1 + e^2)^3} - \frac{3\pi e^4}{(1 + e^2)^4} \left[{}_2F_1\left(\frac{5}{2}, 1; 3; \frac{e^2}{(1 + e^2)} \right) - \frac{1}{2}\, {}_2F_1\left(\frac{3}{2}, 2; 3; \frac{e^2}{(1 + e^2)} \right) \right]. \tag{A7}$$

After additional algebraic manipulation, this result equals the left-hand side of the original equation (eq. [A3]).

REFERENCES

Duncan, M., Quinn, T., & Tremaine, S. 1989, Icarus, 82, 402
Goldreich, P., Lithwick, Y., & Sari, R. 2004a, ApJ, 614, 497
———. 2004b, ARA&A, 42, 549
Goldreich, P., & Tremaine, S. 1980, ApJ, 241, 425
Hindmarsh, A. C., Brown, P. N., Grant, K. E., Lee, S. L., Serban, R., Shumaker, D. E., & Woodward, C. S. 2005, ACM Trans. Math. Software, 31, 363
Ida, S., & Makino, J. 1992, Icarus, 96, 107
Kenyon, S. J., & Bromley, B. C. 2006, AJ, 131, 1837
Kenyon, S. J., & Luu, J. X. 1998, AJ, 115, 2136
Kokubo, E., & Ida, S. 1996, Icarus, 123, 180
Lee, M. H. 2000, Icarus, 143, 74
Ohtsuki, K., Stewart, G. R., & Ida, S. 2002, Icarus, 155, 436
Petit, J.-M., & Henon, M. 1986, Icarus, 66, 536
Rafikov, R. R. 2003, AJ, 125, 942
———. 2004, AJ, 128, 1348
Wetherill, G. W., & Stewart, G. R. 1989, Icarus, 77, 330
———. 1993, Icarus, 106, 190